

# Structure of HIV-2 reverse transcriptase at 2.35-Å resolution and the mechanism of resistance to non-nucleoside inhibitors

J. Ren<sup>\*†</sup>, L. E. Bird<sup>\*†</sup>, P. P. Chamberlain<sup>\*†‡</sup>, G. B. Stewart-Jones<sup>\*</sup>, D. I. Stuart<sup>\*‡</sup>, and D. K. Stammers<sup>\*‡§</sup>

<sup>\*</sup>Division of Structural Biology, The Wellcome Trust Centre for Human Genetics, The Henry Wellcome Building for Genomic Medicine, University of Oxford, Roosevelt Drive, Oxford OX3 7BN, United Kingdom; and <sup>†</sup>Oxford Centre for Molecular Sciences, New Chemistry Building, South Parks Road, Oxford OX1 3QT, United Kingdom

Edited by Stephen C. Harrison, Children's Hospital, Boston, MA, and approved September 4, 2002 (received for review June 19, 2002)

**The HIV-2 serotype of HIV is a cause of disease in parts of the West African population, and there is evidence for its spread to Europe and Asia. HIV-2 reverse transcriptase (RT) demonstrates an intrinsic resistance to non-nucleoside RT inhibitors (NNRTIs), one of two classes of anti-AIDS drugs that target the viral RT. We report the crystal structure of HIV-2 RT to 2.35 Å resolution, which reveals molecular details of the resistance to NNRTIs. HIV-2 RT has a similar overall fold to HIV-1 RT but has structural differences within the "NNRTI pocket" at both conserved and nonconserved residues. The structure points to the role of sequence differences that can give rise to unfavorable inhibitor contacts or destabilization of part of the binding pocket at positions 101, 106, 138, 181, 188, and 190. We also present evidence that the conformation of Ile-181 compared with the HIV-1 Tyr-181 could be a significant contributory factor to this inherent drug resistance of HIV-2 to NNRTIs. The availability of a refined structure of HIV-2 RT will provide a stimulus for the structure-based design of novel non-nucleoside inhibitors that could be used against HIV-2 infection.**

AIDS | drug resistance | crystallography | polymerase

The reverse transcriptase (RT) of HIV-1 has been one of the main targets for the development of anti-AIDS drugs. Combination therapy involving use of anti-RT drugs together with protease inhibitors has led to diminished mortality rates from AIDS in Western countries. HIV-2 is a distinctive HIV serotype that is less widely disseminated than HIV-1. Individuals infected with HIV-2 can go on to develop AIDS but generally do so after a longer clinical latency period than that for HIV-1 (1). HIV-2 infection is thought to have an overall lower morbidity rate than HIV-1, although certain individuals can be more susceptible (2). HIV-2 is most commonly found in certain areas of West Africa, but there is some evidence of a spread of the virus into other geographical regions such as Western Europe (3) and Asia (4). Although HIV-2 RT shows significant amino acid sequence homology to HIV-1 RT, it has marked differences in inhibition by non-nucleoside reverse transcriptase inhibitors (NNRTIs). Additionally, there are differences in kinetic parameters for both the polymerase and RNaseH activities (5), and HIV-2 RT forms a more stable p68/p55 heterodimer compared with the p66/p51 HIV-1 RT heterodimer (6, 7). NNRTIs are structurally diverse hydrophobic molecules that are largely specific for HIV-1 RT, most compounds being completely inactive against HIV-2 RT (8). NNRTIs inhibit HIV-1 RT by binding to an allosteric site  $\approx 10$  Å from the polymerase active site, which results in the distortion of the key catalytic aspartic acid residues (9, 10). Nucleoside analogue inhibitors of RT (NRTIs) such as zidovudine and lamivudine in their 5'-triphosphate forms act as DNA chain terminators and generally have a broad spectrum of antiviral activity that includes HIV-2 as well as HIV-1 (11). Studies of chimeric HIV-1/HIV-2 RTs have indicated some general regions that contribute to the lack of binding of the "first generation" NNRTI nevirapine to HIV-2 RT (12). Some current

combination therapies for HIV-1 infection include NNRTI drugs, either nevirapine, delavirdine, or efavirenz. Such regimens would be less effective for treating HIV-2 infection, and thus NNRTI drugs active against this serotype would be desirable. A few examples of inhibition of HIV-2 RT by NNRTIs are known, but such inhibition tends to be orders of magnitude weaker than for HIV-1 RT. Thus, the NNRTI phenylethylthiazolylthiourea (PETT)-2 inhibits HIV-2 RT with an  $IC_{50}$  of 2  $\mu$ M, whereas the corresponding value for HIV-1 RT is 5 nM (13). Kinetic evidence indicates that PETT-2 does not compete with template-primer or dNTP, consistent with it binding to HIV-2 RT at an equivalent to the HIV-1 RT NNRTI site (13).

Although there are numerous crystal structures of HIV-1 RT published, including complexes with inhibitors (14–16), DNA (17, 18), and unliganded structures (9, 19, 20), there have been no crystal structures reported for HIV-2 RT. A number of examples of high level expression and purification of HIV-2 RT have been published (5, 6, 21), yet these preparations apparently have yielded neither crystals nor structures for this enzyme.

We report here the crystal structure of HIV-2 RT, which has been refined to a resolution of 2.35 Å. The availability of this structure will provide a rational framework for the design of non-nucleoside inhibitors active against HIV-2.

## Materials and Methods

**Protein Purification, Crystallization, and Data Collection.** Cloning, expression, purification, and crystallization of HIV-2 RT (from the pROD isolate, but containing a mutation of Arg286Ser) were as described (22). Briefly, crystals were grown by sitting drop vapor diffusion from droplets consisting of equal volumes of 12 mg/ml HIV-2 RT and 40% ammonium sulfate, either unbuffered or with 0.1 M Tris (pH 8.5). Crystals grew in the presence or absence of 0.7 mM PETT-2, 10% glycerol, or up to 20% DMSO, and were equilibrated briefly in combined adjacent droplets not containing crystals, to which further glycerol was added, giving a final concentration of 20% (vol/vol) before being frozen directly in an Oxford Cryosystems Cryostream for data collection at 100 K at synchrotron sources. The beamlines used were as follows: station PX14.2 at SRS Daresbury (Synchrotron Radiation Source Daresbury, Warrington, Cheshire, U.K.; Dataset 1); station ID14-EH2 at ESRF (European Synchrotron Radiation Facility, Grenoble, France; Dataset 2). In the latter case, data from two separate crystals were merged. Data frames of 1° were recorded on ADSC-q4 (Area Detector Systems

This paper was submitted directly (Track II) to the PNAS office.

Abbreviations: RT, reverse transcriptase; NNRTI, non-nucleoside RT inhibitor; PETT, phenylethylthiazolylthiourea.

Data deposition: The atomic coordinates and structure factors for the 2.35-Å resolution HIV-2 RT structure have been deposited in the Protein Data Bank, www.rcsb.org (PDB ID code 1MU2).

<sup>†</sup>J.R., L.E.B., and P.P.C. contributed equally to this work.

<sup>§</sup>To whom correspondence should be addressed. E-mail: daves@strubi.ox.ac.uk.

**Table 1. Statistics for crystallographic structure determinations**

Data set	1	2
Data collection site	SRS PX14.2	ESRF ID14-EH2
Wavelength, Å	0.979	0.933
Unit cell ( <i>a</i> , <i>b</i> , <i>c</i> in Å)	151.9, 111.9, 82.5	149.8, 107.8, 82.2
Resolution range, Å	25.0–3.30	30.0–2.35
Observations	112,302	631,721
Unique reflections	21,667	56,142
Completeness, %	99.5	100
<i>I</i> / $\sigma$ <i>I</i>	5.2	16.0
<i>R</i> <sub>merge</sub> *	0.239	0.128
Outer resolution shell		
Resolution range, Å	3.42–3.30	2.43–2.35
Unique reflections	2,072	5,520
Completeness, %	97.9	100
<i>I</i> / $\sigma$ <i>I</i>	1.3	1.1
Refinement statistics:		
Resolution range, Å		30.0–2.35
No. of reflections (working/test)		53236/2838
<i>R</i> factor <sup>†</sup> ( <i>R</i> <sub>working</sub> / <i>R</i> <sub>free</sub> )		0.189 (0.194/0.241)
No. of atoms (protein/water/others)		7,744/284/160
rms bond length deviation, Å		0.0081
rms bond angle deviation, °		1.39
Mean <i>B</i> factor, Å <sup>2</sup>		50/58/48/107
rms backbone <i>B</i> -factor deviation <sup>§</sup>		4.5

\**R*<sub>merge</sub> =  $\sum |I - \langle I \rangle| / \sum I$ .

<sup>†</sup>*R* factor =  $\sum |F_o - F_c| / \sum F_o$ .

<sup>‡</sup>Mean *B* factor for main-chain, side-chain, water, and other molecules (sulfate and glycerol), respectively.

<sup>§</sup>rms deviation between *B*-factors for bonded main-chain atoms.

Corporation, San Diego) charge-coupled device (CCD) detectors. HIV-2 RT crystals belong to the orthorhombic space group *P*2<sub>1</sub>2<sub>1</sub>2<sub>1</sub>, with a single heterodimer in the asymmetric unit, and showed variations in unit cell dimensions (Table 1). Data were processed with DENZO and SCALEPACK (23).

**Structure Solution and Refinement.** The HIV-2 RT structure was solved by molecular replacement with the program CNS (24) using coordinates for the unliganded HIV-1 RT heterodimer 1hmV (19). The structure was refined by using CNS, with positional, simulated annealing and individual *B*-factor refinement with bulk solvent correction and anisotropic *B*-factor scaling. Model building was carried out by using O. Coordinates for HIV-1 and HIV-2 RT were overlapped using SHP (25). Statistics for the refined structures are shown in Table 1.

## Results and Discussion

**Structure Determination of HIV-2 RT.** Of a range of HIV-1 RT coordinate sets tested as search molecules for the molecular replacement, the unliganded structure (19) was successful in producing a solution using HIV-2 RT data to 3.3-Å resolution (Dataset 1, see Table 1). The limited resolution of these data allowed partial refinement of the structure (*R*<sub>work</sub> of 0.36). Subsequent growth of better quality crystals of HIV-2 RT led to a higher resolution dataset to 2.7 Å, against which the HIV-2 RT coordinates from Dataset 1 were refined (*R*<sub>work</sub> of 0.187, data not shown). Finally, larger crystals were obtained, which allowed the collection of high-resolution data (2.35 Å, Dataset 2), and the model was refined to an *R* factor of 0.189 (*R*<sub>work</sub>/*R*<sub>free</sub> of 0.194/0.241) with the retention of good stereochemistry (Table 1). Electron density was of excellent quality (Fig. 1A) and clear for the majority of the polypeptide chain except for breaks at

residues 1–2, 68–71, 357–358, and 556–559 in the p68 subunit and 1–5, 92–94, 212–228, and 432 onwards in p55. Dataset 1 gave no convincing electron density for PETT-2 despite the inclusion of this inhibitor in the cocrystallization, and thus HIV-2 RT preferentially crystallizes as the unliganded form under the conditions used. Although the HIV-2 RT crystals have the same space group and similar unit cell dimensions to our HIV-1 RT crystals (26, 27), the molecular packing in the crystals is different, resulting in the central RNA/DNA binding cavity being open to solvent for HIV-2 RT while it is blocked in the HIV-1 RT crystals by the p51 thumb domain from a symmetry-related molecule. Neither the presence of the Arg286Ser mutation (in either p68 or p55) nor the truncated C-terminal region of p55 appear to be near crystal contacts and thus do not apparently directly contribute to the formation of these high-resolution crystals of HIV-2 RT.

**Overall Fold of HIV-2 RT and Comparison with HIV-1 RT.** The subunit and domain organization of the HIV-2 RT p68/p55 heterodimer is shown in Fig. 1B and C. The domain structure of HIV-2 RT p68/p55 corresponds to that of the p66/p51 HIV-1 RT heterodimer (14, 15, 18, 19). There are five domains in the larger subunit, the first three (termed fingers, palm, and thumb) are arranged as in a right hand and are followed by the connection and C-terminal RNaseH domains (14). The smaller subunit lacks the RNaseH domain, and the four remaining domains are disposed differently and more tightly packed than for the p68 subunit. In our model, the p55 subunit ends at residue 431, which agrees with mass spectrometry, suggesting that, as well as truncation of the C-terminal region, there are five residues absent from the N terminus (22). The thumb domain of the p68 subunit adopts a folded down conformation (Fig. 1B and C) similar to that seen in crystals grown of the unliganded HIV-1 RT (19, 20), resulting in a partial occlusion of the cleft, which explains why the initial molecular replacement models of HIV-1 RT containing a more extended thumb domain conformation did not give the correct solution. The thumb domain of the p68 of HIV-2 RT is rotated by 8°, 37°, and 48° relative to unliganded (19), DNA/dNTP-bound (17) and nevirapine-bound (15) HIV-1 RTs, respectively, after the overlap of the whole molecules. Detailed comparison confirms that the greatest similarity of HIV-2 RT to an HIV-1 RT is indeed with the unliganded structure (19) where 720 residues can be superimposed with an rms deviation in C $\alpha$  positions of 1.6 Å.

**Comparison of the NNRTI Site in HIV-1 RT with the Equivalent Region of HIV-2 RT.** The NNRTI site in HIV-1 RT is positioned within the palm domain of the p66 subunit, and a comparison of this with the structurally equivalent region of HIV-2 RT (both as unliganded states) is shown in Fig. 2A. For HIV-1 RT, the presence of a bound NNRTI leads to some conformational rearrangements; for example, the side chains of two residues of the pocket, Tyr-181 and Tyr-188, rotate upwards through  $\approx 120^\circ$ . For HIV-2 RT, it can be seen that, despite amino acid sequence differences, the overall structure of this region is maintained, and the rms deviations for  $\alpha$ -carbons for the overlap of 110 HIV-1 and HIV-2 residues surrounding the NNRTI site is 1.1 Å. Residues that are involved in NNRTI contacts in HIV-1 RT include 95, 100–103, 106, 138 (P51), 179, 181, 188, 190, 224–225, 227, 229, 234–236, and 318. There are numerous changes in the nature of the side chains of these regions: Lys101Ala, Val106Ile, Val179Ile, Tyr181Ile, Tyr188Leu, Gly190Ala, Glu224Asp, His235Trp, and Glu138Ala (p55) (HIV-1 relative to HIV-2). These amino acid substitutions not only lead to significant changes in side-chain bulk but also in electrostatic properties; thus, in two cases there is a change of a positive to neutral charge and in one a change from negative to neutral charge (28). The sequence differences at the two key tyrosine residues 181 and 188 of HIV-1 RT do not

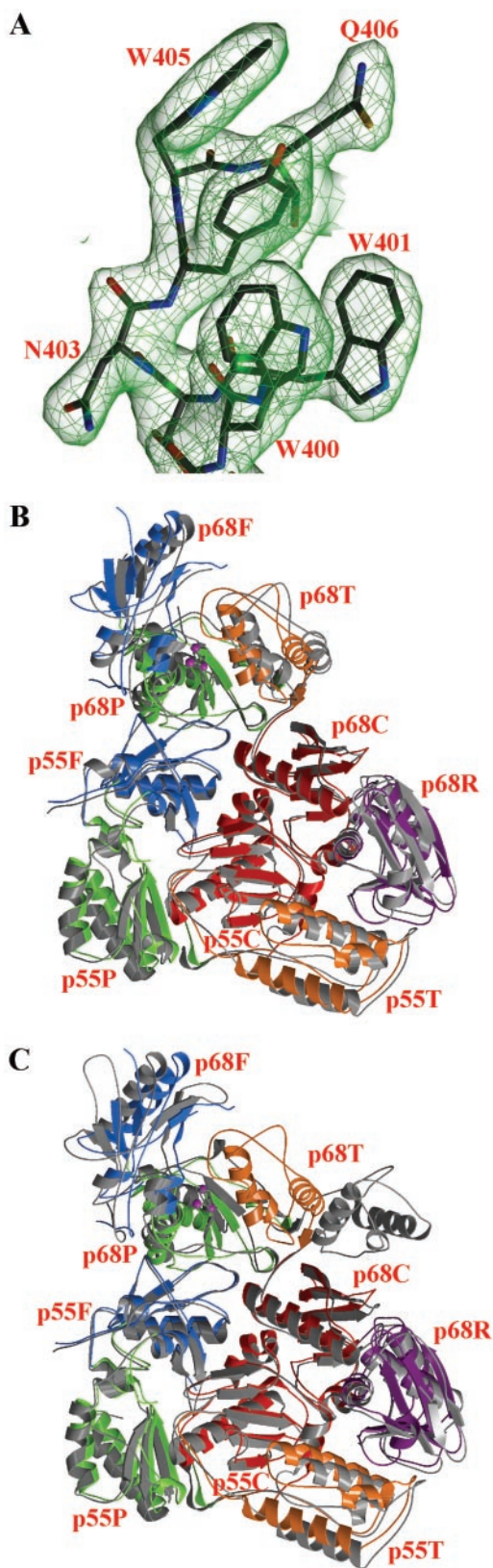


**Fig. 1.** (A)  $2|F_o| - |F_c|$  electron density map contoured at  $1\sigma$  showing residues from 400 to 406 in p68 of HIV-2 RT. (B) Ribbon diagram showing the overall fold of HIV-2 RT overlapped with unliganded HIV-1 RT (1hmv); the HIV-1 RT is shown in gray, and the domains of HIV-2 RT are colored as follows: fingers, blue; palm, green; thumb, orange; connection, red; and RNase H, purple. (C) Ribbon diagram showing the overall fold of HIV-2 RT overlapped with the HIV-1 RT/nevirapine complex (1rtv); the color scheme is as in B.

lead to large shifts in main-chain positions (deviation in  $\alpha$ -carbon positions of 0.5 and 0.4 Å, respectively). Indeed, some conserved residues show larger differences; for example, the  $C\alpha$  of Leu-100 moves by 1.0 Å, with side-chain CG atoms displaced by 2.5 Å (Fig. 2A). For the conserved Trp-229 residue, the  $C\alpha$  is displaced by 1.3 Å from its position in HIV-1 RT. The structural differences in this region appear somewhat larger than earlier suggestions and include main-chain movements (28).

At residue 235, the main chain forms part of the NNRTI site, and there is a change from His (HIV-1 RT) to Trp (HIV-2 RT), resulting in a widening of this region of the pocket in HIV-2 RT, which is in contrast to an earlier suggestion that the marked difference in the binding potency for PETT-1 and PETT-2 compounds (which differ only by a chlorine or nitrile substituent on a pyridine ring) to HIV-2 RT could partly be explained by a narrowing of the NNRTI pocket at this point (13). It is thus possible that PETT-2 binds to HIV-2 RT in a somewhat different mode to that observed for HIV-1 RT.

#### Structural Basis for Resistance of HIV-2 RT to NNRTIs: Evidence from the p68 Subunit.

The determination of the structure of HIV-2 RT allows us to attempt to rationalize its inherent drug resistance to the NNRTIs. First, it should be noted that, although the structure of the binding site is not grossly dissimilar between HIV-1 and HIV-2 RTs, there are alterations in the positions of some conserved residues (e.g., Leu-100) that could in turn perturb potential NNRTI binding. There are also significant side-chain differences between HIV-2 and HIV-1 RT. Although Tyr181Ile and Tyr188Leu retain similar locations in the two structures, the loss of both aromatic side chains results in the abolition of ring stacking interactions with many inhibitors. Such interactions are a major contribution to the binding energy of first generation NNRTIs such as nevirapine to HIV-1 RT (12, 29–31). Inhibition data for chimeric HIV-1/HIV-2 RTs (12) indicate that additional amino acids in the region of 179–189 also contribute to NNRTI binding. However, even these residues do not fully account for all of the difference in affinity for nevirapine. In particular, we have to consider those residues in the 100–106 region, which also interact with NNRTIs. The change of Val106Ile mimics a mutation observed in HIV-1 RT where it confers drug resistance to UC-781 (32). The result of this change in HIV-2 RT is that the isoleucine side chain extends a further 2.8 Å into the pocket, potentially blocking some NNRTIs. The Lys101Glu mutation in HIV-1 RT gives resistance to NNRTIs such as GW420867X (33). In HIV-2 RT, this residue is an alanine, which shows the same trend in size and electrostatic properties as seen for the drug resistance mutation in HIV-1. Residue 101 is positioned at the edge of the NNRTI pocket in HIV-1 RT and can hydrogen bond to Glu-138 in the adjacent p51 subunit, effectively sealing off one side of the pocket from solvent. Mutation of Glu138Arg or Glu138Lys (in p51 of HIV-1 RT) gives resistance to certain NNRTIs, including PETT compounds (34). Residue 138 in HIV-2 RT is alanine, a change to a less bulky uncharged side chain compared with HIV-1 RT. The changes to alanine residues at both positions 101 and 138 would result in greater access for solvent, presumably destabilizing the pocket and weakening inhibitor binding. A further consequence of these changes is the creation of a cavity that in our HIV-2 RT structure is occupied by a glycerol molecule and a sulfate ion (Fig. 2C). A further change in a residue flanking the NNRTI pocket occurs at position 108, which is changed from valine to isoleucine in HIV-2 RT, a known drug resistance mutation in HIV-1 RT (35). Although not in direct contact with NNRTIs, this 108 mutation is thought to exert an effect indirectly via residue 188 which is itself different in HIV-2 RT. Finally, Gly-190 can form a close contact with some NNRTIs such as nevirapine (14, 15), and, although the Gly190Ala change is not

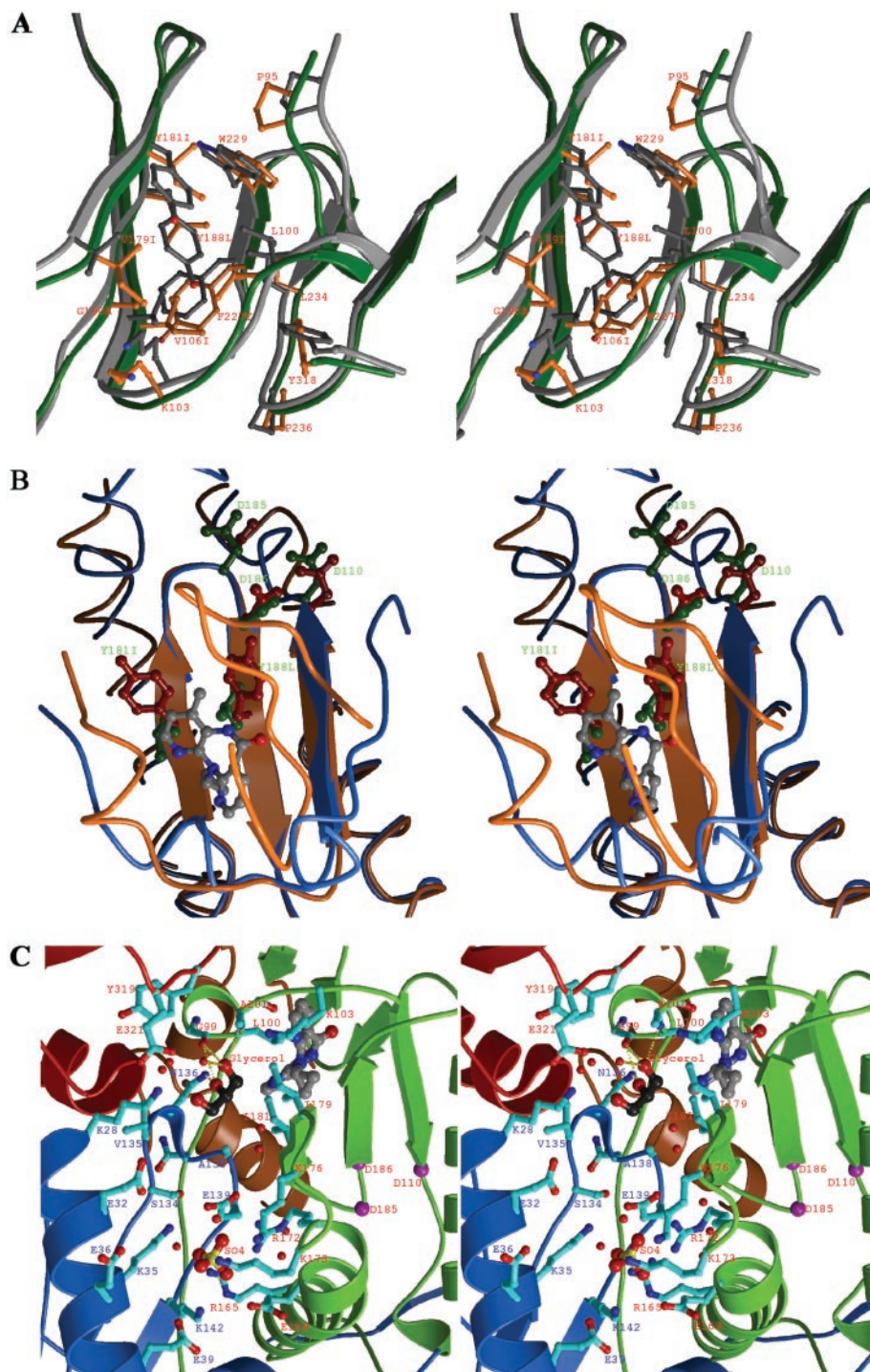


**Fig. 2.** (A) Stereo diagram comparing the NNRTI site of an unliganded HIV-1 RT and the corresponding region of HIV-2 RT. The HIV-1 RT is colored in gray, and the main chain and side chains of HIV-2 RT are shown in green and orange, respectively. (B) Stereo diagram showing part of the HIV-2 RT p55 subunit containing the Ile-181 and Leu-188 side chains (blue and green) overlapped with the corresponding region of the p66 subunit in the nevirapine-bound HIV-1 RT (orange and red). Nevirapine is drawn as ball-and-sticks and colored by atoms. (C) Stereo diagram showing a cavity located at the junction of the p68 palm, p68 connection, and p55 fingers domains (ribbon and coils colored in green, red, and blue, respectively). Side chains of the residues lining the cavity, a bound glycerol and a sulfate are shown in ball-and-stick representation, and are colored by atoms, with carbon atoms in cyan for the side chains and black for the glycerol. Water molecules in the cavity are shown as small red spheres. Larger red spheres label the  $C_{\alpha}$  position of the three catalytic Asp residues at the polymerase active site. Nevirapine colored in gray is shown to mark the NNRTI site in HIV-1 RT. The dashed yellow sticks indicate the four H-bonds from the glycerol to the carbonyl oxygen of Gly-99, the main-chain nitrogen of Ala-101, and a water molecule.

a known resistance mutation in HIV-1 RT, it would cause a steric clash with certain NNRTIs.

In addition to simply mapping the HIV-2 mutations into the

NNRTI binding pocket, we must also address the question of whether conformational changes required for the formation of an NNRTI binding site would be structurally feasible in HIV-2

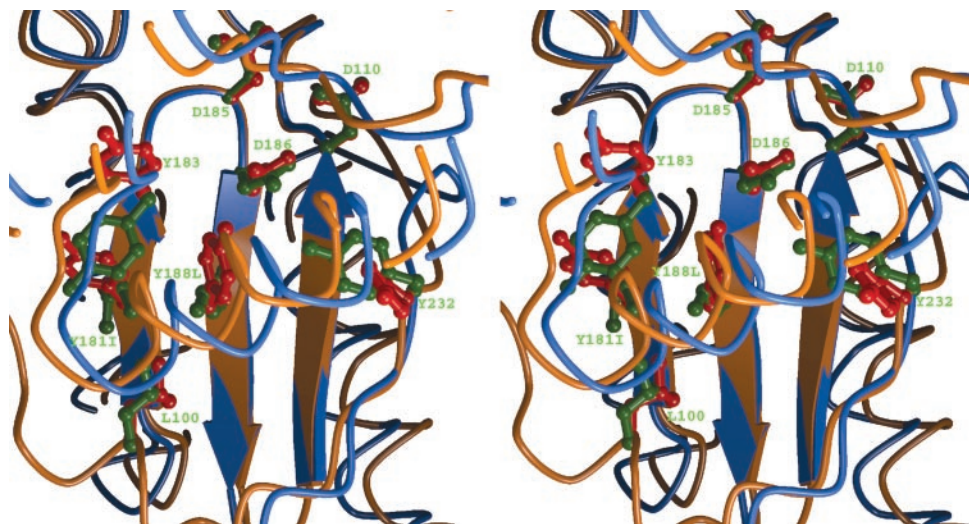


**Fig. 3.** Comparison of the structure around residues 181 and 188 of the p55 subunit in HIV-2 RT with that of p51 subunit in HIV-1 RT. The main chains are shown as ribbons and coils, and side chains as ball-and-stick representations, with HIV-1 RT colored orange and red, and HIV-2 RT blue and green.

RT. We have previously shown that the structural mechanism for the inhibition of HIV-1 RT by NNRTIs is via a distortion of the active site aspartates (9). This rearrangement appears directly linked to the formation of the NNRTI pocket in which Tyr-181 and Tyr-188 undergo a transition from a “down” to an “up” position. The presence of the same architecture for the polymerase active sites of HIV-1 and HIV-2 RTs means that the  $\beta$ -sheet ( $\beta_4$ ,  $\beta_7$ , and  $\beta_8$ ) containing the key catalytic aspartate residues has no apparent barrier to the movement seen in HIV-1 RT resulting from the binding of an NNRTI in the adjacent pocket. We show from the results reported here that, for the unliganded state, the overall structure for the NNRTI binding region is similar but not identical between HIV-1 and HIV-2 RT.

**Structural Basis for Resistance of HIV-2 RT to NNRTIs: Evidence from the Inactive p55 Subunit.** We are fortunate that some features of the p66 NNRTI binding site can, for HIV-1 RT, be inferred in the absence of ligands by examining the corresponding region in the inactive p51 subunit of HIV-1 RT. Thus, we previously noted that this region adopts a very similar conformation to the pocket with an NNRTI bound in the p66 subunit, with both Tyr-181 and Tyr-188 in the up position characteristic of the NNRTI bound state (9). Because both of these residues in HIV-2 RT are much more compact, the question arises of how an energetically unfavorable void is overcome in the p55 subunits. In fact, the stabilization is achieved through some rather modest rearrangements, the two major changes being in the tyrosine residues conserved between HIV-1 and HIV-2 RTs (Tyr-183 and Tyr-232), which swing around to occupy the cavity formed in the vicinity of Ile-181 and Leu-188 (Fig. 3). Residue 183 may be in a somewhat strained conformation because there is also evidence in the electron density for a second minor conformation. The conformation of 181 and 188 themselves also differ between the p68 and p55 subunits; Leu-188 adopts an up position and has a similar  $\chi_1$  value to Tyr-188 of HIV-1 RT ( $-33$  and  $-68^\circ$ , respectively). Despite this similarity in  $\chi_1$  value, the leucine side chain projects into the space that would be occupied by an NNRTI due to its branched aliphatic stereochemistry. Ile-181 is not in a fully up position ( $\chi_1 = 100$  and  $173^\circ$ ), and together with its branched aliphatic side chain, means it projects more into the volume of the binding site, occupied by NNRTIs in HIV-1 RT (Fig. 2*B*). It would thus seem unlikely that first generation NNRTIs could be located

in the pocket in an analogous way to that in HIV-1 RT, and this appears to be a significant contributing factor to the lack of potency for this class of NNRTI binding to HIV-2 RT. The second generation NNRTI efavirenz has some interaction with Tyr-188 yet has minimal contact with Tyr-181 (36, 37), in contrast to nevirapine (14, 15), and these differences in interactions could explain in part why the mutant Leu188Tyr HIV-2 RT has significant sensitivity to efavirenz but not to nevirapine (38). By contrast, delavirdine, which is classed as a first generation NNRTI but has no contact with Tyr-181 in HIV-1 RT (39), can strongly inhibit Leu188Tyr HIV-2 RT (38). Intriguingly PETT-2, a first generation NNRTI with close ring stacking interactions with Tyr-181 in HIV-1 RT (13), retains significant inhibitory potency against wild-type HIV-2 RT, perhaps indicating a different binding mode in HIV-2 RT.

**Design of Non-Nucleoside Drugs Active Against HIV-2 RT.** We have seen that the structure of the NNRTI pocket in HIV-2 RT is more constricted than in HIV-1 RT. However, there is some residual volume that might accommodate potential inhibitors, which would be likely to be significantly different to those tailored for HIV-1 RT. The less bulky side chains at positions 138(p55) and 101 in HIV-2 RT create a potential binding site that is occupied in our structure by a glycerol molecule (Fig. 2*C*). We suggest that other drug-like molecules could be designed to fit this site. Although occupation of this pocket would not distort the catalytic aspartates, it might inhibit relative domain movements because it is positioned at the boundary of the p68 palm, p68 connection, and p55 fingers domains. Alternatively, an inhibitor might be designed that spans the  $5 \text{ \AA}$  from this novel site to the NNRTI pocket.

The availability of a high-resolution HIV-2 RT structure determined to  $2.35 \text{ \AA}$  has allowed us to dissect out factors giving rise to the inherent NNRTI resistance of this HIV serotype. Although the changes in the chemical nature and conformation at residues Ile-181 and Leu-188 probably contribute most to this resistance, differences such as at 101, 106, 108, 138, and 190 also appear significant. The challenge now will be to use structural information to allow the design of novel inhibitors that target HIV-2 RT, which might not only lead to more effective therapies against this HIV serotype but also could help in the development of non-nucleoside inhibitors active against reverse transcriptases from a broader range of human retroviral pathogens.

We thank the staff of the Daresbury Synchrotron Radiation Source (Warrington, Cheshire, U.K.) and the European Synchrotron Radiation Facility (Grenoble, France). We thank the United Kingdom Medical

Research Council for long-term funding of the RT project with grants to D.K.S. and D.I.S. Support from the European Union through Grant QLKT-2000-0029 (to D.K.S.) is also acknowledged.

1. Whittle, H., Morris, J., Todd, J., Corrah, T., Sabally, S., Bangali, J., Ngom, P. T., Rolfe, M. & Wilkins, A. (1994) *AIDS* **8**, 1617–1620.
2. Lucas, S. B., Hounnou, A., Peacock, C., Beaumel, A., Djomand, G., N'Gbichi, J. M., Yeboue, K., Honde, M., Diomande, M., Giordano, C., *et al.* (1993) *AIDS* **7**, 1569–1579.
3. Cilla, G., Rodes, B., Perez-Trallero, E., Arrizabalaga, J. & Soriano, V. (2001) *AIDS Res. Hum. Retroviruses* **17**, 417–422.
4. Kim, S. S., Kim, E. Y., Park, K. Y., Suh, S. D., Park, H. K., Shin, Y. O., Bae, M. & Lee, J. S. (2000) *Acta Virol.* **44**, 15–22.
5. Hizi, A., Tal, R., Shaharabany, M. & Loya, S. (1991) *J. Biol. Chem.* **266**, 6230–6239.
6. Fan, N., Rank, K. B., Poppe, S. M., Tarpley, W. G. & Sharma, S. K. (1996) *Biochemistry* **35**, 1911–1917.
7. Divita, G., Rittinger, K., Restle, T., Immendorfer, U. & Goody, R. S. (1995) *Biochemistry* **34**, 16337–16346.
8. De Clercq, E. (1993) *Med. Res. Rev.* **13**, 229–258.
9. Esnouf, R., Ren, J., Ross, C., Jones, Y., Stammers, D. & Stuart, D. (1995) *Nat. Struct. Biol.* **2**, 303–308.
10. Spence, R. A., Kati, W. M., Anderson, K. S. & Johnson, K. A. (1995) *Science* **267**, 988–993.
11. De Clercq, E. (1994) *Biochem. Pharmacol.* **47**, 155–169.
12. Shih, C. K., Rose, J. M., Hansen, G. L., Wu, J. C., Bacolla, A. & Griffin, J. A. (1991) *Proc. Natl. Acad. Sci. USA* **88**, 9878–9882.
13. Ren, J., Diprose, J., Warren, J., Esnouf, R. M., Bird, L. E., Ikemizu, S., Slater, M., Milton, J., Balzarini, J., Stuart, D. I. & Stammers, D. K. (2000) *J. Biol. Chem.* **275**, 5633–5639.
14. Kohlstaedt, L. A., Wang, J., Friedman, J. M., Rice, P. A. & Steitz, T. A. (1992) *Science* **256**, 1783–1790.
15. Ren, J., Esnouf, R., Garman, E., Somers, D., Ross, C., Kirby, I., Keeling, J., Darby, G., Jones, Y., Stuart, D. & Stammers, D. (1995) *Nat. Struct. Biol.* **2**, 293–302.
16. Ding, J., Das, K., Tantillo, C., Zhang, W., Clark, A. D. J., Jessen, S., Lu, X., Hsiou, Y., Jacobo-Molina, A., Andries, K., *et al.* (1995) *Structure (London)* **3**, 365–379.
17. Huang, H., Chopra, R., Verdine, G. L. & Harrison, S. C. (1998) *Science* **282**, 1669–1675.
18. Jacobo-Molina, A., Ding, J. P., Nanni, R. G., Clark, A. D. J., Lu, X., Tantillo, C., Williams, R. L., Kamer, G., Ferris, A. L., Clark, P., Hizi, A., Hughes, S. H. & Arnold, E. (1993) *Proc. Natl. Acad. Sci. USA* **90**, 6320–6324.
19. Rodgers, D. W., Gamblin, S. J., Harris, B. A., Ray, S., Culp, J. S., Hellmig, B., Woolf, D. J., Deboucq, C. & Harrison, S. C. (1995) *Proc. Natl. Acad. Sci. USA* **92**, 1222–1226.
20. Hsiou, Y., Ding, J., Das, K., Clark, A. D., Jr., Hughes, S. H. & Arnold, E. (1996) *Structure (London)* **4**, 853–860.
21. Muller, B., Restle, T., Kuhnle, H. & Goody, R. S. (1991) *J. Biol. Chem.* **266**, 14709–14713.
22. Bird, L. E., Chamberlain, P. C., Stewart-Jones, G., Ren, J., Stuart, D. I. & Stammers, D. K. (2002) *Protein Expression Purif.*, in press.
23. Otwinowski, Z. & Minor, W. (1996) *Methods Enzymol.* **276**, 307–326.
24. Brunger, A. T., Adams, P. D., Clore, G. M., Delano, W. L., Gros, P., Grosse, K. R. W., Jiang, J. S., Kuszewski, J., Nilges, M., Pannu, N. S., *et al.* (1998) *Acta Crystallogr. D* **54**, 905–921.
25. Stuart, D. I., Levine, M., Muirhead, H. & Stammers, D. K. (1979) *J. Mol. Biol.* **134**, 109–142.
26. Stammers, D. K., Somers, D. O. N., Ross, C. K., Kirby, I., Ray, P. H., Wilson, J. E., Norman, M., Ren, J. S., Esnouf, R. M., Garman, E. F., *et al.* (1994) *J. Mol. Biol.* **242**, 586–588.
27. Esnouf, R. M., Ren, J., Garman, E. F., Somers, D. O. N., Ross, C. K., Jones, E. Y., Stammers, D. K. & Stuart, D. I. (1998) *Acta Crystallogr. D* **54**, 938–954.
28. Tantillo, C., Ding, J., Jacobo-Molina, A., Nanni, R. G., Boyer, P. L., Hughes, S. H., Pauwels, R., Andries, K., Janssen, P. A. J. & Arnold, E. (1994) *J. Mol. Biol.* **243**, 369–387.
29. Hsiou, Y., Das, K., Ding, J., Clark, A. D., Kleim, J.-P., Rosner, M., Winkler, I., Riess, G., Hughes, S. H. & Arnold, E. (1998) *J. Mol. Biol.* **284**, 313–323.
30. Das, K., Ding, J., Hsiou, Y., Clark, A. D., Moereels, H., Koymans, L., Andries, K., Pauwels, R., Janssen, P. A., Boyer, P. L., *et al.* (1996) *J. Mol. Biol.* **264**, 1085–1100.
31. Ren, J., Nichols, C., Bird, L., Chamberlain, P., Weaver, K., Short, S., Stuart, D. I. & Stammers, D. K. (2001) *J. Mol. Biol.* **312**, 795–805.
32. Buckheit, R. W., Jr., Hollingshead, M., Stinson, S., Fliakas-Boltz, V., Pallansch, L. A., Roberson, J., Decker, W., Elder, C., Borgel, S., Bonomi, C., *et al.* (1997) *AIDS Res. Hum. Retroviruses* **13**, 789–796.
33. Balzarini, J., De Clercq, E., Carbonez, A., Burt, V. & Kleim, J. P. (2000) *AIDS Res. Hum. Retroviruses* **16**, 517–528.
34. Zhang, H., Vrang, L., Backbro, K., Lind, P., Sahlberg, C., Unge, T. & Oberg, B. (1995) *Antiviral Res.* **28**, 331–342.
35. Schinazi, R. F., Larder, B. A. & Mellors, J. W. (2000) *Int. Antiviral News* **8**, 65–91.
36. Ren, J., Milton, J., Weaver, K. L., Short, S. A., Stuart, D. I. & Stammers, D. K. (2000) *Structure Fold. Des.* **8**, 1089–1094.
37. Young, S. D., Britcher, S. F., Tran, L. O., Payne, L. S., Lumma, W. C., Lyle, T. A., Huff, J. R., Anderson, P. S., Olsen, D. B., Carroll, S. S., *et al.* (1995) *Antimicrob. Agents Chemother.* **39**, 2602–2605.
38. Isaka, Y., Miki, S., Kawachi, S., Suyama, A., Sugimoto, H., Adachi, A., Miura, T., Hayami, M., Yoshie, O., Fujiwara, T. & Sato, A. (2001) *Arch. Virol.* **146**, 743–755.
39. Esnouf, R. M., Ren, J., Hopkins, A. L., Ross, C. K., Jones, E. Y., Stammers, D. K. & Stuart, D. I. (1997) *Proc. Natl. Acad. Sci. USA* **94**, 3984–3989.